Iranian Journal of Geophysics, 2021, Page 89 – 99 (Research)
DOI: 10.30499/ijg.2020.251816.1294

On the Diffusivity of Noise Data Recorded (2-8 Hz) at Stations Located in North-Western Iran

Amir Ali Hamed [1] and Ali Moradi [2]*

[1] *Ph.D Student, Department of Seismology, Institute of Geophysics, University of Tehran, Tehran, Iran*
[2] *Associate Professor, Department of Seismology, Institute of Geophysics, University of Tehran, Tehran, Iran*

(Received: 8 October 2020, Accepted: 15 December 2020)

Abstract

Since the advent of seismic interferometry, the cross-correlation of received random noises has been very frequently used for the approximate assessment of the empirical Green's function between the station pairs. Theoretically, the diffusivity of noise wavefield is the key factor that contributes to the success of this idea in real applications. Diffusivity itself requires the fulfillment of two conditions of energy equipartitioning as well as a homogeneous distribution of the incoming noise. To meet these requirements, the attempts are made to select a longer study period to homogenize the incoming azimuths. This solution is mostly logical in the range of 0.1-0.3 Hz, because it is believed that in this frequency range, microseismic noise waves are received continuously by the stations. But at higher frequencies, seismic sources are mostly changing both spatially and temporally, and their spectral content is not stationary over time. Therefore, in high-frequency seismic interferometry, prolonging the study interval will not help much in improving the signal-to-noise ratio of the retrieved Green's functions. For this reason, the main focus in such studies is on highly heterogeneous regions because multiple scattering in these regions may be able to azimuthally homogenize the wave field to some extent. According to the scientific studies, however, the homogeneity of the azimuthal distribution of noise is very unlikely to happen, even in the most heterogeneous areas. So to know which claim is more correct, we turned our attention to the northwestern region of Iran, where the severe heterogeneity of the medium for frequencies above 1 Hz has already been confirmed by recent studies. With the help of a Frequency-Dependent Polarization Analysis (FDPA), we first extracted those elliptically polarized waves whose degree of polarization (IDOP) was greater than 0.8. This constraint assures us that the received waves have maintained their coherency for a relatively long time before reaching the station. Our analysis on the azimuths of these polarized data fail to pass Kuaper and U^2 tests, indicating that the azimuth distribution of the received signals at the stations located in north-western Iran is azimuthally inhomogeneous. At the stations near the topography, even strong directivity in coherent seismic noises was observed.

Keywords: Seismic noise interferometry, Diffusivity, Azimuthal homogeneity

*Corresponding author: asmoradi@ut.ac.ir

1 Introduction

Seismic interferometry is a revolutionary field of a research that offers an innovative basis to obtain the approximate assessment of the empirical Green's function (i.e. EGF) between the station pairs, simply by cross-correlating received random seismic noises (for a comprehensive review, see Wapenaar et al. 2010a,b; Campillo & Roux 2014; Nakata et al., 2019 and references therein). In general terms, the availability of a diffuse wavefield is a prerequisite to implementing this method in real applications (e.g. Hodgson 1996; Hennino et al., 2001; Weaver & Lobkis 2006; Sánchez-Sesma et al., 2008). Theoretically, for a system to be called a perfect diffuse system, it has to follow the theorem of the energy equipartitioning. Moreover, the azimuthal distribution of the noise in a diffuse system is homogeneous. To fill this gap in the studies performed at microseismic frequency bandwidth (0.1-0.3 Hz), the processing time is usually extended (e.g. several years). The reasoning behind this extension is that azimuths of the incoming noises generally tend to become uniform with extending the processing interval. But, extending the processing interval does not necessarily fulfill the conditions required for executing the seismic interferometry in the frequency range higher than 1 Hz. This is because high-frequency seismic waves are mainly generated from non-reproducible and short-lived sources, and *t*heir stationarity interval is usually just in the order of less than one minute (e.g. 3-24 s) (Gorbatikov & Stepanova 2008). In response to this concern, researchers are constantly trying to find new reproducible high-frequency seismic sources in seismic interferometry. The preconditions stated above are generally deemed to be fulfilled at the stage of the isotropically developed multiple scattering processes in a heterogeneous medium or a finite medium with an irregular bounding surface (e.g. Margerin et al., 2009; Pilz & Parolai 2014). But the other studies have the opposite view and believe that *the* azimuthal isotropy hypotheses are never met in "real environments world" operating (Mulargia et al., 2010; Mulargia 2012; Afonin et al., 2019; Liu & Ben-Zion 2018). To make sure that these ideas can be effectively put into practice, this study intends to test whether the homogeneous distribution of the azimuth noise is observed at the stations located in the northwestern region of Iran or not.

2 The Study Region and datasets

The location of stations and their surrounding landscapes are depicted in Figureure. (1). These stations invoked our interest because according to the studies conducted by Nagavi et al., (2017), the north-western region of Iran, especially the areas where the stations are located, are generally very heterogeneous. These stations belong to the Iranian Seismological Centre, Institute of Geophysics, University of Tehran (IRSC-IGUT, http://irsc.ut.ac.ir). They recorded data in the Nanometrics Y-File format in a 50 Hz sampling rate. Available data from which the analysis was carried out included different-length fragments. We removed the instrumental response from all of the fragments to obtain the ground velocity data. Thereafter, they were baseline corrected and were merged to obtain 24-hour-length continuous data (Figureure. 2a). All data-logger-induced spikes and glitches zeroed out by Seismic Analysis Code (Figureure. 2b). Signals were bandpass filtered using a fourth-order causal Butterworth filter to isolate the part of the signals that lies within the frequency bandwidth a (2-8) Hz.

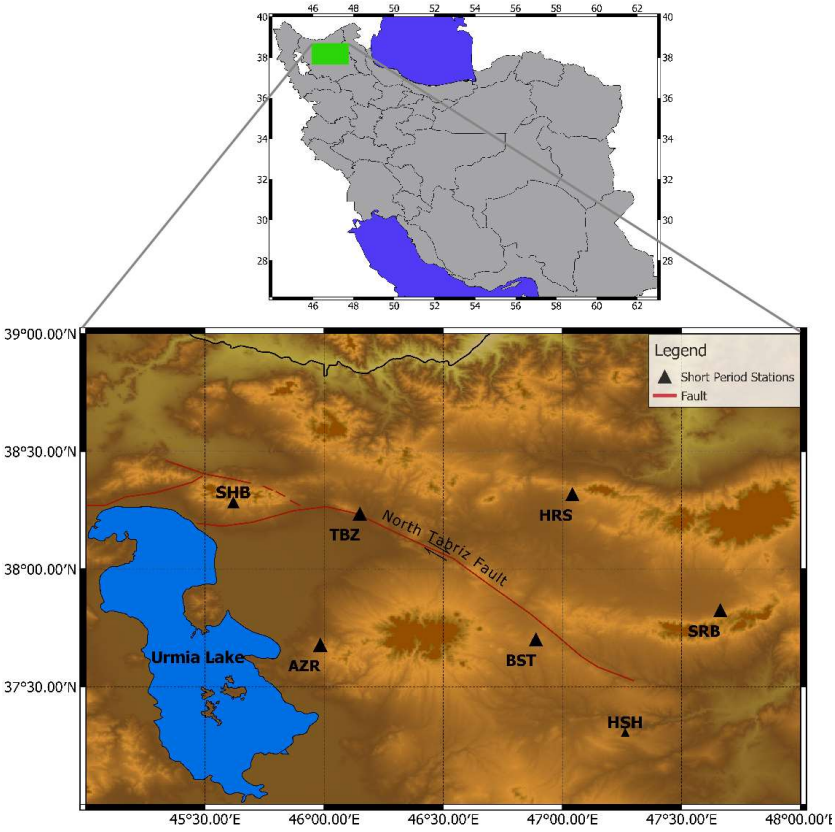

Figure 1. The black triangles show the location of stations used in this study.

(a)

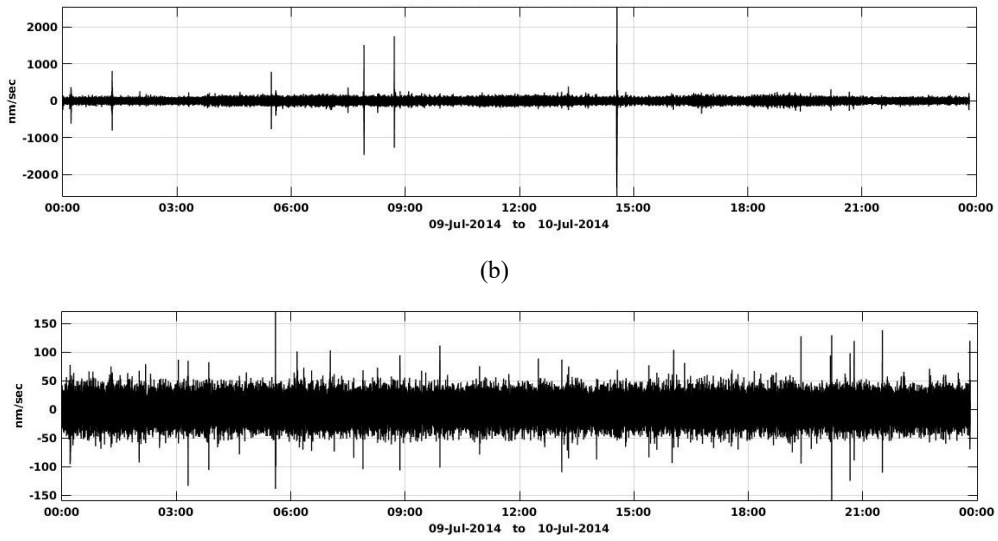

(b)

Figure 2. a) The 24-hour continues seismic data, b) the 24-hour continues data after removing the data-logger-induced spikes and glitches.

3 Frequency-Dependent Polarization Analysis

Tracking the particle trajectories of a medium, also known as the polarity analysis, is a more straightforward approach to unravel the directional properties of seismic wavefields. There are several different ways for the polarity analysis, but the Frequency-Dependent Polarization Analysis (FDPA) has hitherto been successfully utilized to both seismic noise and earthquake data (Schimmel & Gallart 2003; 2004; Schimmel et.al, 2011). In line with this strategy, an adaptive-length Gaussian-shaped sliding window moves along the three-component data vector, $\vec{x}(t)^T = [x_1(t), x_2(t), x_3(t)]$. A "snapshot" is taken at a defined period in time in such a way that the length of each snapshot becomes equal to the smallest instantaneous period of the three components. The cross-spectral matrix for each snapshot over the frequency range of $(2\delta + 1)$ Hz would therefore be returned as

$$\mathbf{S}(t, f) = \frac{1}{2\delta+1} \sum_{k=f-\delta}^{f+\delta} \vec{\zeta}(t, f)\, \vec{\zeta}(t, f)^{\dagger} \qquad (1)$$

where † stands for the conjugate complex and $\vec{\zeta}(t, f)$ is

$$\vec{\zeta}(t, k) = \sum_{\tau=t-T(f)/2}^{t+T(f)/2} \Pi(t - \tau)\, \vec{x}(\tau) \exp(-ik\tau) \qquad (2)$$

In this equation, the $\Pi(.)$ indicates Gaussian-shaped windows and T stands for the length of the sliding windows. As usual, the spectral matrixes are decomposed into their eigenvalues, $\lambda_i(t, f), i = 1,2,3,$ and corresponding eigenvectors, $\vec{v}_i(t, f), i = 1,2,3,$ to simplify more complex matrix operations. The condition under which $\lambda_1(t, f) \gg \lambda_2(t, f), \lambda_3(t, f)$ are called the pure state. This condition is a matter of special concern, because in this condition the semi-major, $\vec{a}(t, f)$, and semi-minor, $\vec{b}(t, f)$ attributes are determined just from the eigenvector associated with the largest eigenvalue, that is, λ_1. The Instantaneous Back-Azimuth (IBAZ) values of motion ellipses, $\varphi(t, f)$, can be determined in terms of these attributes (see Schimmel & Gallart 2004 for details). To analyze and characterize the elliptically polarized signals, we divided the total 24-hour-length continuous data into two-hour length time intervals. Then, in each 10-minute interval, we selected 180-second time windows from these time intervals. In these 180-second windows, we performed the polarization analysis.

Recent studies show that seismic waves at frequencies above 1 Hz are mainly composed of Rayleigh surface waves (Koper et al., 2010; Koper & Hawley 2010). In their fundamental mode, these Rayleigh waves propagate almost exclusively in a retrograde particle motion at the surface of the Earth (Aki & Richards, 1980). The retrograde assumption for the motions helps us to resolve the $180°$ ambiguity in determining the IBAZs. But it should not be forgotten that higher mode surface waves beside the fundamental mode can also be present at the higher frequencies. The higher mode Rayleigh waves may propagate in either retrograde or prograde motions. To isolate sections of the time series in which retrograde motion dominates, therefore, we applied the polarity mute method introduced by Gribler et al., (2016). Figure. (3) shows the polarization spectra obtained for the SRB station at each two-hour length of the day. All the polarization spectra clearly show a multimodal distribution. We saw similar results for the other stations.

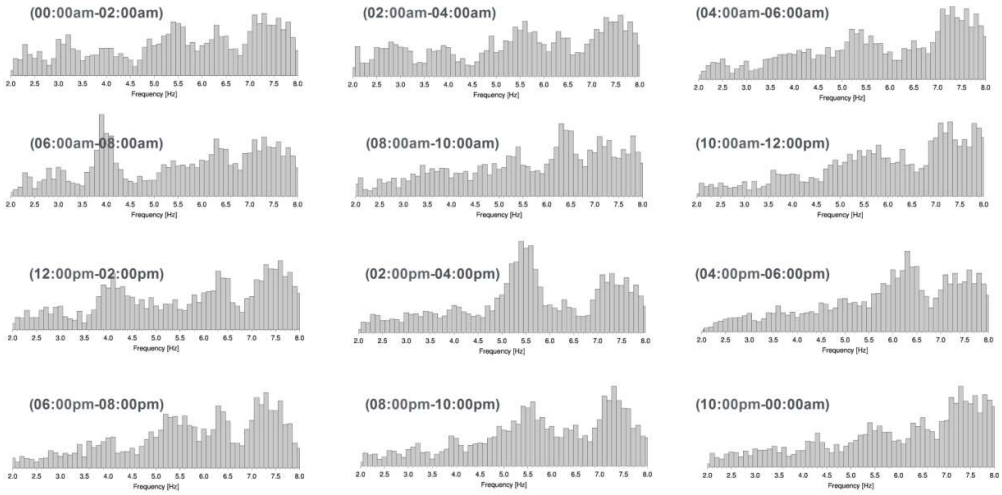

Figure 3. Polarization spectra obtained for the SRB station at each two-hour length of the day. All the polarization spectra clearly show a multimodal distribution.

4. Instantaneous Degree-of-polarization

Unquestionably, a considerable part of the retrieved IBAZs is most likely emitted from the sources that have rapid fluctuations as a function of frequency/time. However, Schimmel et al., (2011) showed that we will be able to come to a decision on the moments when the IBAZs are related to steadily polarized waves with the aid of the Instantaneous Degree-of-Polarization (IDOP) of motions, $\vec{p}(t,f)$. This parameter reveals the variation of the planarity vectors of the polarized signals with respect to the mean direction of these vectors as

$$\mathrm{DOP}(t,f) = \left[\frac{1}{N(f)}\sum_{\tau=t-T(f)/2}^{t+T(f)/2}\left|\frac{\vec{m}(t,f)}{|\vec{m}(t,f)|}\cdot\frac{\vec{p}(\tau,f)}{|\vec{p}(\tau,f)|}\right|^{\beta_1}\right]^{\beta_2} \quad (3)$$

where $\vec{p}(t,f) = \vec{a}(t,f)\otimes\vec{b}(t,f)$ denotes the planarity vector and the sign $\otimes$ stands for the vectorial cross product. The planarity vector is the perpendicular vector to the instantaneous plane of the ground motion ellipse. The following equation is used to determine the mean vector $\vec{m}$ within the instantaneous sliding window, T,

$$\vec{m}(t,f) = \frac{1}{N(f)}\sum_{\tau=t-T(f)/2}^{t+T(f)/2}\frac{\vec{p}(\tau,f)}{|\vec{p}(\tau,f)|}, \quad (4)$$

where the $N(f)$ indicates the total number of samples in each window, and the positive β_1 and β_2 exponents control the sensitivity of this method by increasing the differences between polarized and less polarized signals. In this paper, we fixed their values in $\beta_1 = \beta_2 = \beta = 2$.

The IDOP changes in a range between 0 and 1. In the cases in which the semi-major axis direction is strongly varying, it is expected to have a smaller value for the IDOP, while for a perfectly polarized motion the IDOP will be 1. We used a rose diagram as a tool to display the results obtained for DOP in a polar coordinate. These diagrams comprise 16 radiating spokes" around the circle. The length of each "spoke' is related to the amount of

elliptically polarized signals detected at each station from a particular azimuth. Each concentric circle represents a different frequency in the occurrence, starting from zero at the center to the increasing occurrence frequencies at the outer circle. Each spoke is broken into discrete categories that show the percentage of time that waves with a particular IDOP are received from a particular as a function of their instantaneous IDOP. We only kept the measurements corresponding to stable instantaneous elliptical polarization within the frequency-dependent sliding polarization analysis window. This sliding window is taken to be equal to a time period of a minimum of four times of the signal period. Detections were based on IDOP larger than 0.8 which is shown in the dark red colour in hourly processing results (Figure 4a). This constraint assures us that the received waves have maintained their coherency for a relatively long time before reaching the station.

5 Test on the homogeneity of the azimuthal distribution of noise

In general, different methods have been offered to check if these data include some sort of departure from evenness or not. Mulargia (2012) showed that the Kuaper's test (Mardia & Jupp, 1999, Section 6.3; Mulargia 2012) and the modified version of a U^2-test in the azimuthally binned form of data (Choulakian et al., 1994) have a superior power to analyze the degree of departure of seismic circular data from uniformity. The procedure for these two methods is as follows. First, those azimuths for which the amplitude is greater than zero (i.e. $[\Theta_1, \Theta_2, \dots, \Theta_N]$) are multiplied into their associated intensity and arranged into the monotonically ascending order as $[\alpha_1, \alpha_2, \dots, \alpha_N]$, $i = 1, \dots, N$. The basic ingredient of this approach is the use of the following null hypothesis: H_0: The underlying distribution of the incoming noise wavefield is isotropic, in comparison with its counterpart non-isotropic assumption, that is: H_1: There are unknown number of unknown predominant orientations for incoming noise wavefield. Accordingly, the proposed Kuaper's test amounts to compare the empirical cumulative distribution function of these sorted data, Γ, and the one corresponds to a purely uniform distribution to decide about the uniformity of data. Suppose D^+ and D^- are obtained from the following equations

$$D^+ = \max\left|\frac{i}{N} - \Gamma(\alpha_i)\right|, D^- = \max\left|\Gamma(\alpha_i)\frac{(i-1)}{N}\right| \quad (5)$$

With this assumption, the Kuiper's critical value, $\mathcal{K}$, will obey from

$$\mathcal{K} = V_n\left(N^{\frac{1}{2}} + 0.155 + \frac{0.24}{N^{\frac{1}{2}}}\right),$$

where

$$V_n = D^+ + D^- \quad (6)$$

If the incoming noise wavefield happens to be isotropic, $\mathcal{K}$ is expected to take a value smaller than the upper tail percentage points given at Stephens, (1970), for different levels, whereas exceeding this threshold leads to rejecting the hypothesis of the azimuthal isotropic wavefield.

(a)

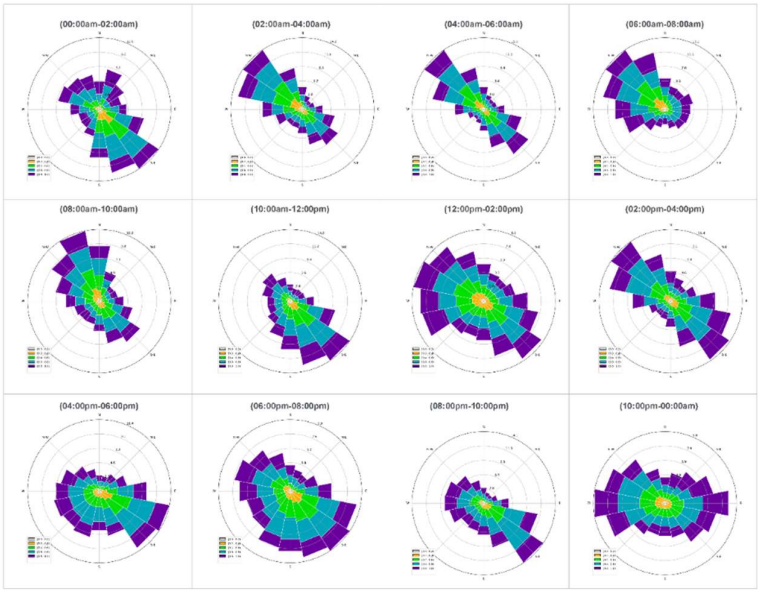

(b)

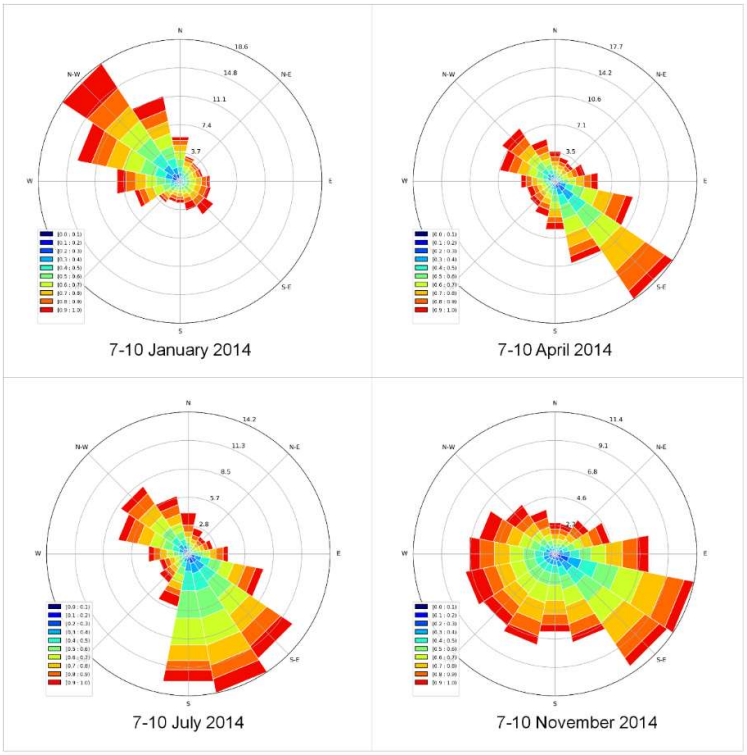

Figure 4. a) We used a rose diagram as a tool to display the results in a polar coordinate for the SRB station at each two-hour length of the day. These diagrams comprise 16 radiating spokes" around the circle. The length of each "spoke' is related to the amount of elliptically polarized signals detected at each station from a particular azimuth. Each concentric circle represents a different frequency in the occurrence, starting from zero at the center to increasing occurrence frequencies at the outer circle. Each spoke is broken into discrete categories that show the percentage of time that waves with a particular IDOP are received from a particular as a function of their instantaneous IDOP. These categories are: Grey [0-0.2], Orange [0.2-0.4], Green [0.4-0.6], Blue [0.6-0.8], and Purple [0.8-1.0]. b) Seasonal variations of the three-day average of combined polarity data in the SRB station.

U^2 test is another method to evaluate the homogeneity of the noises. In this test, we classified the azimuthal data into the $J = 36$ azimuthal bins and labeled them by $1, 2, \ldots, 36$ sequential numbers with the 10° azimuthal intervals. This approach can also be used for analyzing the uniformity in the multimodal distributions (Jones 2006). For an isotropic wavefield, U^2 test take a value smaller than the upper tail percentage points given at Choulakian et al., (1994, Table 1) for different levels, otherwise, it can confidently reject the hypothesis of the isotropic wavefield. To estimate the p-values of significance tests and its confidence interval, we resampled the original data to generate $N_R = 1000$ samples. Then, we separately reiterate the uniformity evaluation for all samples, belonging to the regenerated and the original data. The p-values of significance tests can be defined as the proportion of these $N_R + 1$ values of the test statistic that are at least as extreme as the test statistic value for the original data (Pewsey et al., 2013, p. 9-10).

Table 1. The values returned by Kuaper's and U^2 test.

Station	Testing on the uniformity by Kuaper's test	Testing on the uniformity by U^2 test
AZR	(23.1)	(0.4853)
BST	(31.4)	(0.5884)
HRS	(26.5)	(0.5773)
HSH	(31.1)	(0.4646)
SHB	(18.5)	(0.4589)
SRB	(25.7)	(0.5052)
TBZ	(14.3)	(0.4416)

All tests give P-value < 0.01 so this test emphatically fails to pass the null hypothesis of uniformity at the 1% significance level for all stations.

Table (1) shows a typical example of a test performed on 2-hour data at all stations. According to the results, in all cases, azimuthal data fail to pass both uniformity tests with a p-value < 0.01, so this test emphatically rejects the null hypothesis of uniformity at the 1% significance level. This failure to pass the homogeneity of the azimuthal distribution of noise indicates that there is no diffusivity condition for any of the stations in northwestern Iran. While these results are consistent with the studies conducted by Mulargia & Castellaro, (2010) and Mulargia, (2012), they are contrary to the results obtained by Pilz & Parolai (2014). Another noteworthy point is that in some stations, including SRB, HRS, and SHB, even a clear directivity was evident in their results. What these stations had in common was that all three were located near the topographic slopes. Directivity in the response of topographic slopes in frequencies above 1 Hz has also been reported in many other studies (Massa et al., 2014; Burjánek et al.,2010; 2014). As can be seen from the three-day average of combined polarity data, the northwest-southeast trend for polarity results at SRB station is unchanged in different seasons of the year (Figure.4b). The dominant azimuths of the polarized data are clear in the frequency-azimuth polarity distribution of SRB, HRS, and HRS stations (Figure 5a). These dominant azimuths are almost visible for three-day polarity analysis as well (Figure 5b). Of course, these dominant frequencies are somewhat lost between large volumes of data, yet there is still no homogeneity in the input intensities of different azimuths.

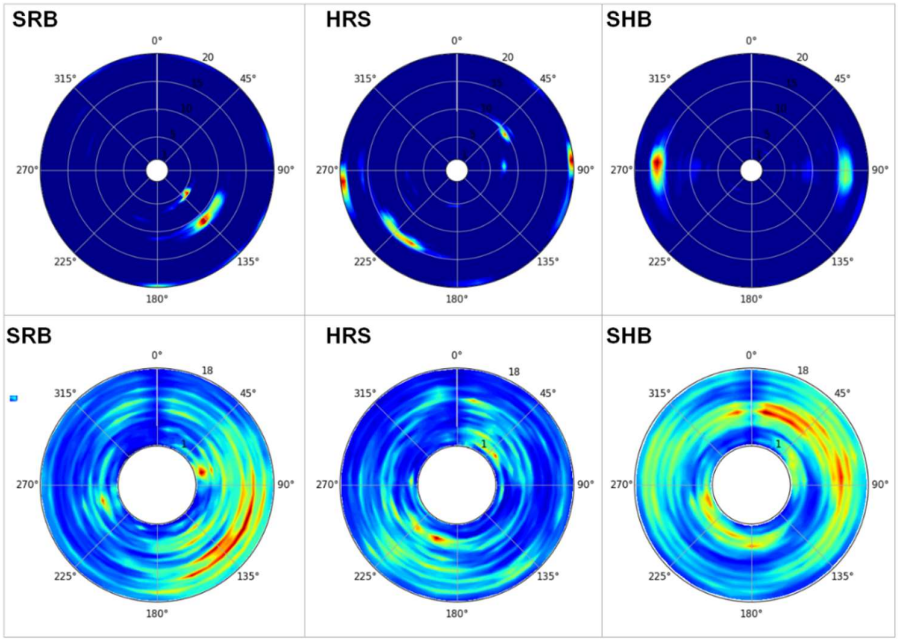

Figure 5. a) The dominant azimuths of the polarized data are clear in the frequency-azimuth polarity distribution of SRB, HRS, and HRS stations. b) These dominant azimuths are almost visible for three-day polarity analysis as well.

5 Conclusion

In this study, the time-frequency instantaneous polarization analysis has been proposed as a simple approach to learning the degree of diffusivity of incoming random noise wavefield at frequencies above 1 Hz in the areas close to the stations in the northwestern region of Iran. To be confirmed about the deviations from the uniformity of these data, we conducted the Kuaper's and U^2 test. All of the data failed to pass these uniformity tests. By relying on this finding, waves with a large degree of polarization (IDOP) don't satisfy the azimuthal homogeneity. Therefore, the heterogeneity of the environment in these regions is not such that the interferometry method can be implemented. However, the observations confirmed that in the stations near the topographic gradients, coherent seismic noises are continuously received in almost constant frequency and azimuth ranges. This result is consistent with a study conducted by Ping et al., (2020) where it is shown that the topographic gradients can be used as direct virtual seismic sources in a high-frequency seismic interferometry.

References

Afonin, N., Kozlovskaya, E., Nevalainen, J., Narkilahti, J., 2019. Improving the quality of empirical Green's functions, obtained by cross-correlation of high-frequency ambient seismic noise. Solid Earth, **10**, 1621-1634.

Burjánek, J., Edwards, B., Fäh, D., 2014. Empirical evidence of local seismic effects at sites with pronounced topography: a systematic approach. Geophysical Journal International 197, 608-619.

Burjánek, J., Gassner-Stamm, G., Poggi, V., Moore, J.R., Fäh, D., 2010. Ambient vibration analysis of an unstable mountain slope. Geophysical Journal International 180, 820-828.

Campillo, M., Roux, P., Romanowicz, B., Dziewonski, A., 2014. Seismic

imaging and monitoring with ambient noise correlations. Treatise on geophysics 1, 256-271.

Choulakian, V., Lockhart, R.A., Stephens, M.A., 1994. Cramér-von Mises statistics for discrete distributions. The Canadian Journal of Statistics/La Revue Canadienne de Statistique, 125-137.

Gorbatikov, A., Stepanova, M.Y., 2008. Statistical characteristics and stationarity properties of low-frequency seismic signals. Izvestiya, Physics of the Solid Earth 44, 50-59.

Gribler, G., Liberty, L.M., Mikesell, T.D., Michaels, P., 2016. Isolating retrograde and prograde Rayleigh-wave modes using a polarity mute. Geophysics 81, V379-V385.

Hodgson, M., 1996. When is diffuse-field theory applicable? Applied Acoustics 49, 197-207.

Koper, K.D., Hawley, V.L., 2010. Frequency dependent polarization analysis of ambient seismic noise recorded at a broadband seismometer in the central United States. Earthquake Science 23, 439-447.

Koper, K.D., Seats, K., Benz, H., 2010. On the composition of Earth's short-period seismic noise field. Bulletin of the Seismological Society of America 100, 606-617.

Liu, X., Ben-Zion, Y., 2018. Analysis of non-diffuse characteristics of the seismic noise field in southern California based on correlations of neighbouring frequencies. Geophysical Journal International 212, 798-806.

Mardia, K.V., Jupp, P.E., 2009. Directional statistics. John Wiley & Sons.

Margerin, L., Campillo, M., Van Tiggelen, B., Hennino, R., 2009. Energy partition of seismic coda waves in layered media: Theory and application to Pinyon Flats Observatory. Geophysical Journal International 177, 571-585.

Massa, M., Barani, S., Lovati, S., 2014. Overview of topographic effects based on experimental observations: meaning, causes and possible interpretations. Geophysical Journal International 197, 1537-1550.

Mulargia, F., 2012. The seismic noise wavefield is not diffuse. The Journal of the Acoustical Society of America 131, 2853-2858.

Mulargia, F., Castellaro, S., 2010. Nondiffuse elastic and anelastic passive imaging. The Journal of the Acoustical Society of America 127, 1391-1396.

Naghavi, M., Rahimi, H., Moradi, A., Mukhopadhyay, S., 2017. Spatial variations of seismic attenuation in the North West of Iranian plateau from analysis of coda waves. Tectonophysics 708, 70-80.

Nakata, N., Gualtieri, L., Fichtner, A., 2019. Seismic ambient noise. Cambridge University Press.

Pilz, M., Parolai, S., 2014. Statistical properties of the seismic noise field: influence of soil heterogeneities. Geophysical Journal International 199, 430-440.

Ping, P., Chu, R., Zhang, Y., Xie, J., 2020. Enhancing Signal-to-Noise Ratios of High-Frequency Rayleigh Waves Extracted from Ambient Seismic Noises in Topographic Region. Bulletin of the Seismological Society of America 110, 793-802.

Richards, P.G., Aki, K., 1980. Quantitative Seismology: Theory and Methods. Freeman.

Sánchez-Sesma, F.J., Pérez-Ruiz, J.A., Luzon, F., Campillo, M., Rodríguez-Castellanos, A., 2008. Diffuse fields in dynamic elasticity. Wave motion 45, 641-654.

Schimmel, M., 1999. Phase cross-correlations: Design, comparisons, and applications. Bulletin of the Seismological Society of America 89,

1366-1378.

Schimmel, M., Stutzmann, E., Ardhuin, F., Gallart, J., 2011. Polarized Earth's ambient microseismic noise. Geochemistry, Geophysics, Geosystems, **12**(7), 1-14.

Schimmel, M., Stutzmann, E., Gallart, J., 2011. Using instantaneous phase coherence for signal extraction from ambient noise data at a local to a global scale. Geophysical Journal International 184, 494-506.

Schimmel, M., Stutzmann, E., Ventosa, S., 2018. Low-frequency ambient noise autocorrelations: Waveforms and normal modes. Seismological Research Letters 89, 1488-1496.

Stephens, M.A., 1970. Use of the Kolmogorov–Smirnov, Cramer–Von Mises and related statistics without extensive tables. Journal of the Royal Statistical Society: Series B (Methodological) 32, 115-122.

Wapenaar, K., Draganov, D., Snieder, R., Campman, X., Verdel, A., 2010. Tutorial on seismic interferometry: Part 1—Basic principles and applications. Geophysics 75, 75A195-175A209.

Wapenaar, K., Slob, E., Snieder, R., Curtis, A., 2010. Tutorial on seismic interferometry: Part 2—Underlying theory and new advances. Geophysics 75, 75A211-275A227.

Weaver, R.L., Lobkis, O.I., 2006. Diffuse fields in ultrasonics and seismology. Geophysics 71, SI5-SI9.